## PAPER

Check for updates

# Effects of growth substrate on the nucleation of monolayer MoTe₂†

David J. Hynek,[a] Raivat M. Singhania,[b] James L. Hart,[a] Benjamin Davis,[b] Mengjing Wang,[a] Nicholas C. Strandwitz[b] and Judy J. Cha [iD] *[a]

The discovery and characterization of two-dimensional (2D) materials beyond graphene has increased dramatically over the past decade with increasingly fine control over the growth dynamics of these materials. $MoTe_2$ represents a model material for studying phase change properties of 2D materials due to small energy differences between its 2H semiconducting phase and 1T′ semimetallic phase. Although some substrates are demonstrated to be better than others for the wafer-scale growth of high quality $MoTe_2$ films, substrate effects on the nucleation and growth of $MoTe_2$ are still not well understood. Here, we grow monolayer $MoTe_2$ by converting $MoO_x$ thin films deposited on three different substrates: sapphire $Al_2O_3$ (0001), amorphous $SiO_2$, and amorphous $AlO_x$, and examine the early stages of the conversion reaction to elucidate the substrate effects on the nucleation of $MoTe_2$. We observe that the chemical composition of the substrate is more important than the surface topography and crystallinity of the substrate, with high quality monolayer 2H $MoTe_2$ formed on both $Al_2O_3$ (0001) and $AlO_x$ in contrast to mixed phase 2H/1T′ $MoTe_2$ formed on $SiO_2$, as determined by Raman spectroscopy, X-ray photoelectron spectroscopy, and atomic force microscopy.

## Introduction

Due to their low-dimensionality and layer-dependent properties, 2D materials have been heavily studied in recent years for their potential applications that range from catalysis[1] to energy storage.[2] Transition metal dichalcogenides (TMDCs) of the form $MX_2$ (M: Mo, W; X: S, Se, Te) represent a particularly heavily studied subset of 2D materials due to the wide variety of electronic phases readily accessible, expanding their uses in next-generation electronics. Of these TMDCs, $MoTe_2$ has gained recent attention for potential applications in phase-change memory and low power electronics due to small free energy differences between its semiconducting 2H (α) phase and semimetallic 1T′ (β) phase at room temperature,[3] and between semimetallic 1T′ (β) phase and topological $T_d$ (γ) phase at low temperatures.[4,5] Many studies have shown useful physical characteristics including superconductivity,[6–8] a possible quantum spin Hall state,[9] and reversible phase switching,[10–12] yet, reliable large-scale

growth of $MoTe_2$ with thickness control and high crystallinity has remained a challenge.

Several physical and electrical characterization studies have been carried out using $MoTe_2$ flakes obtained by exfoliation or chemical vapor deposition (CVD),[8,13,14] but these methods suffer from low yield and a lack of scalability. We have recently demonstrated synthesis of thickness-controlled $MoTe_2$ films through the tellurization of $MoO_x$ ($2 < x < 3$) thin films deposited by atomic layer deposition (ALD), where the number of ALD cycles determined the thickness of the $MoTe_2$ films.[15] The $MoTe_2$ films were uniform across a wafer scale and could be synthesized on $Al_2O_3$ (0001) down to a monolayer. In this work, we examined the effects of substrate composition and structure on the nucleation and crystallinity of $MoTe_2$ thin films when $MoTe_2$ was converted from ALD-deposited $MoO_x$ thin films. To determine how the growth of $MoTe_2$ is affected by the chemical composition or crystallinity of the underlying substrate, we utilized the following substrates: sapphire $Al_2O_3$ (0001), 3 nm-thick ALD-deposited amorphous $AlO_x$ on $SiO_2$/Si, and amorphous $SiO_2$. We show that the complete conversion from $MoO_x$ to monolayer 2H $MoTe_2$ can be achieved on both $Al_2O_3$ (0001) and amorphous $AlO_x$ while only mixed phase 2H/1T′ films were realized on amorphous $SiO_2$. Our results indicate that chemical composition plays a more important role than the crystallinity or surface topography of the growth substrate.

[a] *Energy Sciences Institute, Department of Mechanical Engineering and Materials Science, Yale University, West Haven, CT 06516, USA. E-mail: judy.cha@yale.edu*
[b] *Department of Materials Science and Engineering, Lehigh University, Bethlehem, PA 18015, USA*

# Results and discussion

Amorphous $MoO_x$ films were deposited by ALD on sapphire $Al_2O_3$ (0001), 3 nm-thick ALD-deposited amorphous $AlO_x$, and amorphous $SiO_2$ (Methods). Based on our previous study,[15] $MoO_x$ thin films of 8 and 10 ALD cycles were chosen to grow monolayer $MoTe_2$ in order to maximize the effects of the substrate on the crystalline quality of $MoTe_2$ while a $MoO_x$ film of 120 ALD cycles was used to grow a thick $MoTe_2$ for transmission electron microscopy (TEM) characterization. The oxide films were tellurized in a two-zone furnace under an $H_2$/Ar atmosphere at 600 °C for three different time intervals: 15 minutes, 20 minutes, and 50 minutes (Fig. 1e, see Methods for synthesis details). This 8–10 cycle synthesis resulted in a discontinuous, polycrystalline film (Fig. S1a and b†), where the individual domains consisted of monolayer 2H $MoTe_2$, with an average domain size of 10–20 nm. The discontinuity observed in $MoTe_2$ is due to the fact that 8 and 10 ALD cycle $MoO_x$ films were not sufficiently thick to form a continuous monolayer. Uniform and continuous 2H $MoTe_2$ films were obtained using the 120 ALD cycle $MoO_x$ films deposited on amorphous $AlO_x$ (Fig. 1f and g). The selected area electron diffraction and high-resolution TEM images confirm the 2H phase for $MoTe_2$.

The evolution of the crystalline phase of the $MoTe_2$ films on the three different substrates was tracked throughout the length of the 50 minute reaction after three different time

intervals (15 minutes, 20 minutes, and 50 minutes) using Raman spectroscopy (Fig. 2) (Methods). The 2H phase is characterized by two main modes at 170 $cm^{-1}$ ($A_{1g}$) and 234 $cm^{-1}$ ($E_{2g}^1$),[16–18] while the 1T′ phase is characterized by a primary mode at 163 $cm^{-1}$ ($A_g^4$).[19] For $MoTe_2$ synthesis, it is known that the 1T′ phase is initially synthesized due to the Te-deficient stoichiometry and a 2H phase can nucleate out of the 1T′ phase with the continual supply of Te vapor[3,15] (Fig. S2†). After a 15 minute growth, only the 8 cycle-thick $MoO_x$ film on amorphous $AlO_x$ has converted fully to 2H $MoTe_2$, while the $MoTe_2$ on $Al_2O_3$ (0001) and amorphous $SiO_2$ shows a mixed phase of 2H and 1T′. After 20 minutes of growth, $MoTe_2$ on the $Al_2O_3$ (0001) substrate has also fully converted to 2H, while the $MoTe_2$ on amorphous $SiO_2$ still remains mixed-phase. From 20 to 50 minutes of growth, the growth result did not change substantially, with $MoTe_2$ on the $AlO_x$ and $Al_2O_3$ (0001) substrates remaining in the 2H phase, and $MoTe_2$ on the $SiO_2$ not converting fully to the 2H phase (Fig. 2d). We observe the same trend when 10 cycle-thick $MoO_x$ films were converted to $MoTe_2$ on the three substrates (Fig. S3†).

The progression of the $MoTe_2$ films from $MoO_x$ is further characterized using X-ray photoelectron spectroscopy (XPS) (Fig. 3). Mo has two primary peaks at 228 eV ($3d_{5/2}$) and 231 eV ($3d_{3/2}$),[20] with Mo-oxide peaks at slightly higher binding energies. By tracking the intensity of the oxide peaks as a function of reaction time, the reaction time needed to transform $MoO_x$ to $MoTe_2$ was determined for each substrate. In agreement with the Raman results, after 15 minutes of reaction, $MoTe_2$ converted on the amorphous $AlO_x$ substrate is shown to have the least amount of oxidized Mo. $MoTe_2$ converted on $Al_2O_3$ (0001) and amorphous $SiO_2$ substrates still show significant amounts of Mo-oxide peaks, suggesting incomplete conversion to $MoTe_2$. After 20 minutes of reaction, all films show almost a complete reduction in Mo-oxide peaks, with little change from 20 to 50 minutes of reaction. Interestingly, a residual amount of $MoO_x$ remains in the $MoTe_2$ films converted on the amorphous $SiO_2$ and amorphous $AlO_x$ substrates, with a higher concentration evident in the $SiO_2$ substrate, and no residual oxidation is observed in the $MoTe_2$ converted on sapphire (Fig. 3d). This residual $MoO_x$ may be from surface oxidation of $MoTe_2$, or due to non van der Waals bonding at the interface between $MoTe_2$ and the two amorphous substrates. If the residual $MoO_x$ were from the surface oxidation of $MoTe_2$, the $MoO_x$ peaks should be present for $MoTe_2$ on all three substrates, which is not the case. Thus, the residual $MoO_x$ observed for the two amorphous substrates cannot be attributed to the surface oxidation of $MoTe_2$. This hypothesis is further supported by very little oxidation in the Te peaks for all three substrates after 50 minutes of reaction (Fig. S4†). The absence of the oxide peaks for $MoTe_2$ converted on $Al_2O_3$ (0001) thus suggests that the residual $MoO_x$ is either from the chemical bonds of $MoTe_2$ to the amorphous oxide substrates or from the diffusion of Mo atoms into the amorphous oxide substrates.
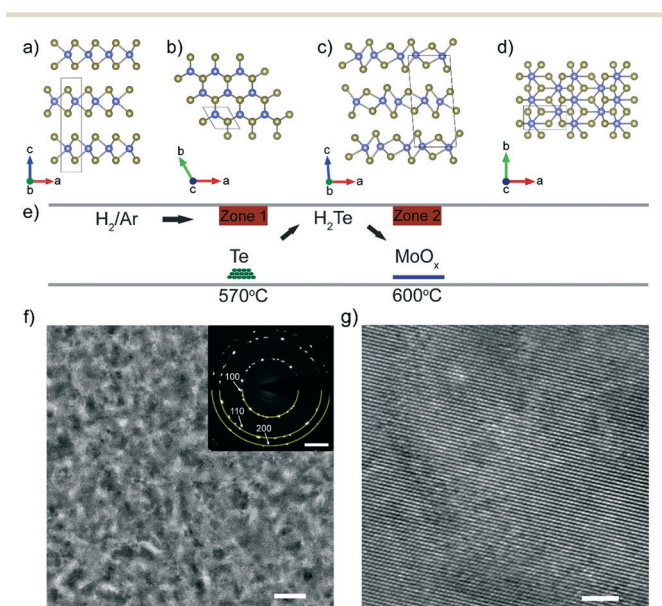


**Fig. 1** Growth of 2H $MoTe_2$ converted from $MoO_x$ thin films. a and b) 2H $MoTe_2$ viewed along *b*- and *c*-axis. c and d) 1T′ $MoTe_2$ viewed along *b*- and *c*-axis. e) Two-zone furnace growth schematic. f) TEM image taken along the *c*-axis, showing a 2H $MoTe_2$ film, converted from 120 ALD cycle-thick $MoO_x$ grown on 3 nm-thick amorphous $AlO_x$. Scale bar, 100 nm. (Inset) selected area electron diffraction from (f). Scale bar, 10 $nm^{-1}$. g) High resolution TEM image of the film shown in (f). Scale bar, 3 nm.
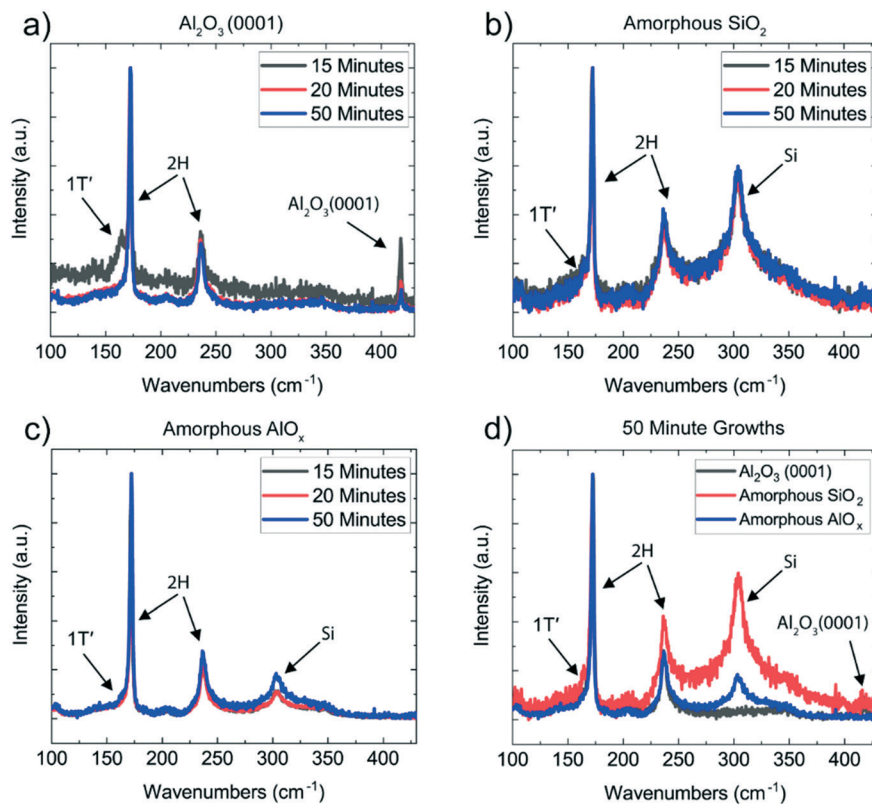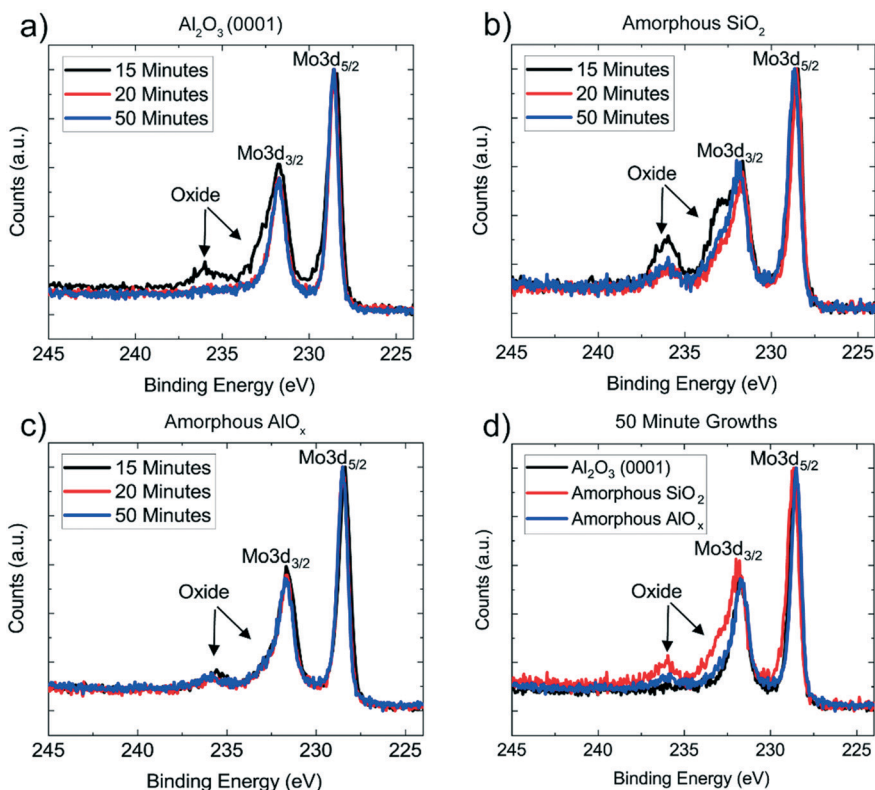
**Fig. 2** Raman spectroscopy characterization of MoTe$_2$ films converted on different substrates at varying reaction times. Raman spectra of MoTe$_2$ converted from 8 cycle-thick MoO$_x$ deposited on Al$_2$O$_3$ (0001) (a), amorphous SiO$_2$ (b), and amorphous AlO$_x$ (c). Spectra were captured after three different intervals for each sample: 15 minutes (black), 20 minutes (red), and 50 minutes (blue). Overlaid spectra from all three substrates after 50 minutes of growth are shown in (d).

We note the residual MoO$_x$ is not reflected in the O 1s binding energy, which is dominated by the oxygen of the underlying substrates (Fig. S5†). The same result is observed when 10 cycle-thick MoO$_x$ films were converted on the three substrates (Fig. S6†).

We also investigated the topography of the MoTe$_2$ films using atomic force microscopy (AFM). Fig. 4 shows the changes in topography of MoTe$_2$ as a function of substrate and reaction time. Before the reaction, the surface roughness of the MoO$_x$ films deposited on the three substrates was measured, showing that the Al$_2$O$_3$ (0001) case is the most flat and films grown on amorphous AlO$_x$ and SiO$_x$ substrates have higher surface roughness similar to each other. No significant changes were observed in the surface roughness after annealing the MoO$_x$ films in H$_2$/Ar environment at 600 °C (Fig. S7†). After the conversion to MoTe$_2$, the height distribution profiles show that the surface roughness of MoTe$_2$ on all three substrates is much larger than the initial surface roughness of the substrates (Fig. 4e, j and o), indicating the formation of discontinuous monolayer MoTe$_2$ islands of domain size in the 10's of nm range (Fig. 4d, i and n). This is due to the insufficient number of ALD cycles for the initial MoO$_x$ precursor film for the synthesis of continuous monolayer MoTe$_2$ and could be remedied by increasing the thickness of the MoO$_x$ film.[15] MoTe$_2$ films converted on

Al$_2$O$_3$ (0001) are the most flat, while MoTe$_2$ films converted on amorphous AlO$_x$ became slightly rougher as the conversion continued from 15 minutes to 50 minutes of reaction time. In contrast, the surface roughness of the MoTe$_2$ on the SiO$_2$ substrate did not appear to change after the initial 15 minutes of reaction and, after 50 minutes of reaction, the surface roughness of the MoTe$_2$ is the largest on SiO$_2$. The same trend in surface roughness was observed for MoTe$_2$ films converted from 10 cycle-thick MoO$_x$ films (Fig. S8†).

The Raman and XPS analysis suggest that MoTe$_2$ conversion occurs most quickly on the amorphous AlO$_x$ substrate and most slowly on the amorphous SiO$_2$ substrate. Additionally, residual MoO$_x$ peaks remain for MoTe$_2$ converted on amorphous substrates, possibly suggesting chemical bonding at the interface between MoTe$_2$ and the substrate. Therefore, from the combination of Raman spectroscopy, XPS, and AFM analysis, we conclude that the chemistry of the substrate has a major role in the nucleation of 2H monolayer MoTe$_2$ films from precursor MoO$_x$ films. One reason this could occur is the overall diffusivity of the MoO$_x$ films on SiO$_2$ $vs.$ AlO$_x$. It has been shown previously that MoO$_x$ shows greater diffusivity on amorphous AlO$_x$ than it does on amorphous SiO$_2$,[21] indicating stronger wetting between MoO$_x$ and AlO$_x$. Growth of other TMDCs on AlO$_x$
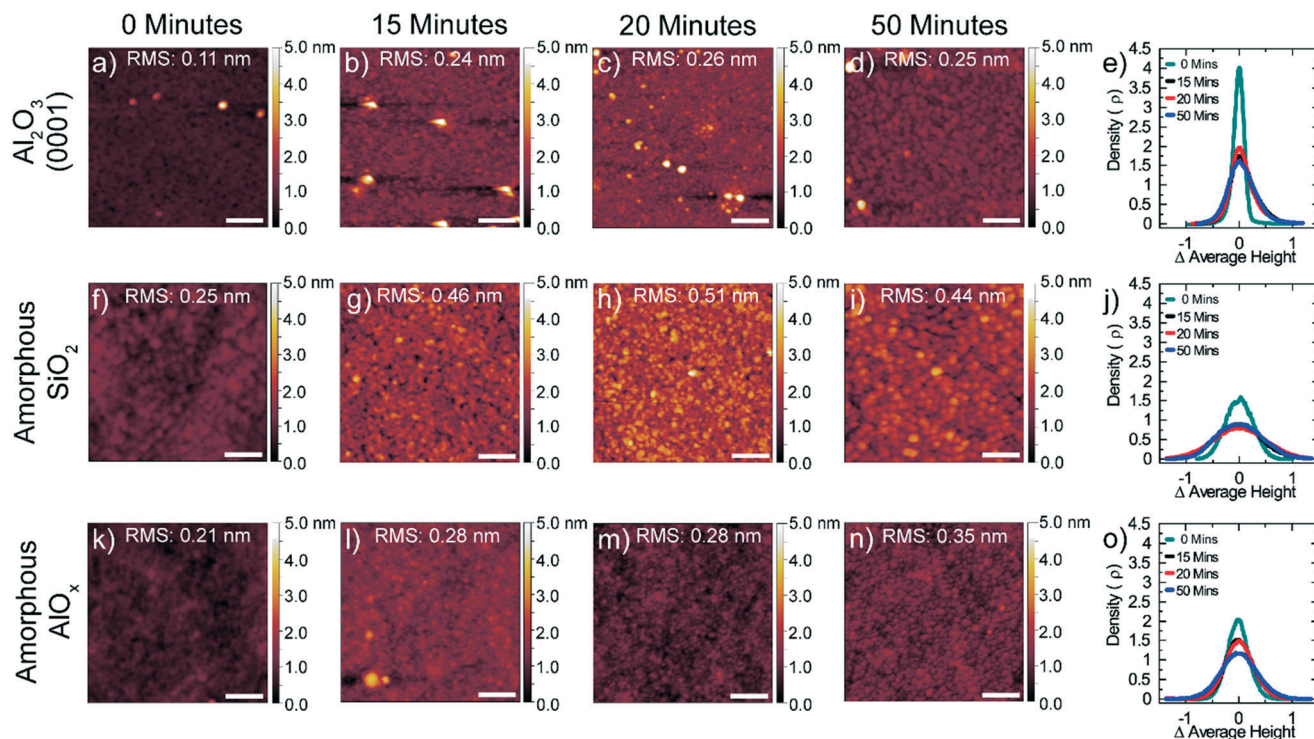
**Fig. 3** XPS analysis of Mo 3d peaks in MoTe$_2$ films converted on different substrates at varying reaction times. XPS of Mo 3d peaks in MoTe$_2$ films converted from 8 cycle-thick MoO$_x$ deposited on Al$_2$O$_3$ (0001) (a), amorphous SiO$_2$ (b), and amorphous AlO$_x$ (c). Spectra were captured after three different intervals for each sample: 15 minutes (black), 20 minutes (red), and 50 minutes (blue). Overlaid spectra from all three substrates after 50 minutes of growth are shown in (d).

and SiO$_x$ substrates has also been examined. When WS$_2$ was synthesized directly on different substrates by ALD using WF$_6$ and H$_2$S as precursors, the Delabie group at University of Leuben showed that WS$_2$ on amorphous AlO$_x$ and sapphire Al$_2$O$_3$ grew in a layer-by-layer manner,[22] while WS$_2$ on amorphous SiO$_2$ grew in a 3D manner as clusters.[23] Their results suggest that the W precursor interacts more strongly with sapphire Al$_2$O$_3$ or AlO$_x$ than with SiO$_2$, similar to the diffusivity case of MoO$_x$ on AlO$_x$ *vs.* SiO$_2$. Additionally, it has been shown that adhesion of metal atoms to oxide supports depends more strongly on the choice of oxide support rather than the metal.[24] Thus, these studies provide strong evidence that the conformal synthesis of 2D materials on AlO$_x$ *vs.* SiO$_x$ substrates is driven by better adhesion between metal atoms (Mo or W) and the oxide substrates underneath, as opposed to crystallinity of the substrates. We also note that strain imparted from the substrate due to different degrees of thermal expansion could stabilize the 1T′ phase over the 2H phase. It has been shown that CVD grown WSe$_2$ on SiO$_2$ experience significant tensile strain due to a large mismatch between the thermal expansion coefficient values, while WSe$_2$ grown on sapphire experience little strain due to similar thermal expansion coefficients.[25] This could be significant as the phase transition of MoTe$_2$ is sensitive to strain.[26] In addition to the effect of substrate composition on the nucleation and film uniformity of MoTe$_2$, we further observe

that substrate crystallinity affects the bonding at the interface between MoTe$_2$ and substrate: MoO$_x$ is present at the interface between MoTe$_2$ and amorphous AlO$_x$ while it is absent between MoTe$_2$ and crystalline Al$_2$O$_3$. Although a relationship has been determined for MoTe$_2$ on the three different substrates, conclusive physical explanations for why adhesion energies of metal atoms on different oxide substrates are different are unclear.[24]

## Conclusion

While large-area synthesis of MoTe$_2$ thin films has been demonstrated previously, the impact of chemistry and crystallinity of the substrate on the nucleation and crystalline quality of MoTe$_2$ has been unclear. Here, we show that the conversion of MoO$_x$ to monolayer 2H MoTe$_2$ proceeds at comparable rates on amorphous AlO$_x$ and Al$_2$O$_3$ (0001), while the conversion is slower on SiO$_2$. We conclude that this is due to increased wetting between Te or Mo atoms on the surface of AlO$_x$ compared to SiO$_x$, allowing for improved lateral mobility and reconfiguration to successfully realize the 2H phase. This work shows the need for further studies regarding substrate interactions during synthesis of 2D materials and for increased understanding of the diffusion of metal species on oxide films.

**Fig. 4** AFM characterization of MoTe$_2$ films converted on different substrates at varying reaction times. AFM images of MoTe$_2$ converted from 8 cycle-thick MoO$_x$ deposited on Al$_2$O$_3$ (0001) (a–d), amorphous SiO$_2$ (f–i), and amorphous AlO$_x$ (k–n) after different reaction times. Scale bars, 100 nm. Height profiles for the three substrates (e, j and o) were obtained by averaging the height distributions of four AFM images taken from each sample, 8 μm distance from one another at each time point: 0 minutes (cyan, pristine oxide), 15 minutes (black), 20 minutes (red), and 50 minutes (blue).

# Methods

### Atomic layer deposition of MoO$_x$ films and substrate preparation

Silicon wet thermal oxide substrates (500 nm, University Wafer) were prepared using a standard RCA process. Samples were immersed in a 5 : 1 : 1 volume ratio solution of deionized (18 MΩ) H$_2$O (18.2 MΩ) : NH$_4$OH : H$_2$O$_2$ and subsequently immersed in a 6 : 1 : 1 solution of DI H$_2$O : HCl : H$_2$O$_2$. Both rinses were conducted for 10 min between 70 and 80 °C and were immediately followed by a DI H$_2$O rinse.

Atomic layer deposition of 3 nm thick AlO$_x$ films was performed in a Cambridge Nanotech S-100 reactor at a substrate temperature of 200 °C. The silicon thermal oxide substrates (500 nm, University Wafer) were first pretreated with UV-ozone for 2 minutes. Trimethylaluminum (TMA) and O$_3$ were utilized as precursors for 30 cycles of ALD, giving approximately 3 nm of amorphous AlO$_x$ on the surface of the thermal oxide substrate.

Sapphire substrates were cleaned in a modified version of the RCA process.[27] The first step was a soak in an ethanol bath for 12 hours at room temperature, followed by a rinse with DI H$_2$O. Samples were then sonicated for 30 min at room temperature in a 1 : 20 : 79 solution of detergent : ethanol : DI H$_2$O. Samples were then soaked in a 3 : 1 H$_2$SO$_4$ : H$_2$O$_2$ piranha solution. Finally, samples were immersed in more concentrated variants of the standard RCA solutions,

comprising 2 : 1 : 1 DI H$_2$O : NH$_4$OH : H$_2$O$_2$ and 2 : 1 : 1 DI H$_2$O : HCl : H$_2$O$_2$. Each of the latter 3 rinses was conducted for 20 min at 80 °C and was followed with a DI H$_2$O rinse. All samples were dried with high purity nitrogen gas between each step.

Atomic layer deposition of MoO$_x$ films was performed in a Cambridge Nanotech S-100 reactor at a substrate temperature of 200 °C. Bis(*tert*-butylimido)bis(dimethylamido)molybdenum (NtBu)$_2$(NMe$_2$)$_2$Mo and ozone were utilized as precursors in accordance with a previously published procedure.[28] Films of different thicknesses were synthesized using cycle numbers of 8, 10, and 120.

### Conversion of MoO$_x$ to MoTe$_2$ films

MoTe$_2$ thin films were synthesized through the annealing of MoO$_x$ thin films of various thicknesses grown by ALD in a tellurium atmosphere. Te powder (2 g, Sigma-Aldrich, 99.999%) was placed in a 2 inch quartz tube at zone 1 of a two-zone furnace (MTI OTF-1200X-II), while MoO$_x$ thin films on various substrates were placed downstream in the second zone of the tube furnace. After purging the tube many times with Ar to ensure no residual oxygen was present, the two zones were heated to 570 °C for Te powder and 600 °C for MoO$_x$ films in 15 min and held there for 50 minutes total, with characterization conducted after 3 different time intervals: 15 minutes, 20 minutes, and 50 minutes. A mixture

of H$_2$/Ar was flowed at 100/10 sccm in atmospheric pressure during the reaction. After the synthesis was completed, the chamber was purged with 200 sccm Ar gas for 25 minutes, and then rapidly cooled to room temperature by opening the furnace cover. We note that the samples were removed from the furnace for characterization between the three time intervals. Thus, the samples were first reacted for 15 minutes, then for additional 5 minutes (denoted as '20 minutes'), and finally for additional 30 minutes (denoted as '50 minutes').

### Structural and chemical characterization

Plan-view TEM images were taken at 200 kV using a Tecnai Osiris microscope at the Yale Institute for Quantum Engineering (YINQE). All plan-view MoTe$_2$ films were grown on amorphous AlO$_x$ substrates for easy lift-off using hydrofluoric acid as etching of sapphire for lift-off was proven difficult and the lifted MoTe$_2$ films were transferred onto carbon covered Quantifoil TEM grids with equally spaced 2 μm holes. To characterize the surface of the films, atomic force microscopy was conducted using a Cypher ES microscope from Asylum Research. The microscope was operated in peak-force tapping mode. Raman spectroscopy (Horiba) was used to verify film uniformity and characterize the thickness and phase of the MoTe$_2$ films. The laser used was 633 nm, with a laser power of 10% and diffraction grating 1800 g mm$^{-1}$. Full conversion of the films from MoO$_x$ to MoTe$_2$ was verified through X-ray photoelectron spectroscopy (XPS) (PHI VersaProbe II).

## Conflicts of interest

There are no conflicts to declare.

## Acknowledgements

## References

1 D. Deng, K. S. Novoselov, Q. Fu, N. Zheng, Z. Tian and X. Bao, Catalysis with Two-Dimensional Materials and Their Heterostructures, *Nat. Nanotechnol.*, 2016, **11**, 218–230.

2 B. Xu, S. Qi, M. Jin, X. Cai, L. Lai, Z. Sun, X. Han, Z. Lin, H. Shao, P. Peng, Z. Xiang, J. E. ten Elshof, R. Tan, C. Liu, Z. Zhang, X. Duan and J. Ma, 2020 Roadmap on Two-Dimensional Materials for Energy Storage and Conversion, *Chin. Chem. Lett.*, 2019, **30**, 2053–2064.

3 X. Xu, S. Chen, S. Liu, X. Cheng, W. Xu, P. Li, Y. Wan, S. Yang, W. Gong, K. Yuan, P. Gao, Y. Ye and L. Dai, Millimeter-Scale Single-Crystalline Semiconducting MoTe$_2$ via Solid-to-Solid Phase Transformation, *J. Am. Chem. Soc.*, 2019, **141**, 2128–2134.

4 Y. Tao, J. A. Schneeloch, C. Duan, M. Matsuda, S. E. Dissanayake, A. A. Aczel, J. A. Fernandez-Baca, F. Ye and D. Louca, Appearance of a T$_d$* Phase across the T$_d$-T′ Phase Boundary in the Weyl Semimetal MoTe$_2$, *Phys. Rev. B*, 2019, **100**, 100101(R).

5 C. Heikes, I. L. Liu, T. Metz, C. Eckberg, P. Neves, Y. Wu, L. Hung, P. Piccoli, H. Cao, J. Leao, J. Paglione, T. Yildirim, N. P. Butch and W. Ratcliff, Mechanical Control of Crystal Symmetry and Superconductivity in Weyl Semimetal MoTe$_2$, *Phys. Rev. Mater.*, 2018, **2**, 074202.

6 Y. Qi, P. G. Naumov, M. N. Ali, C. R. Rajamathi, W. Schnelle, O. Barkalov, M. Hanfland, S.-C. Wu, C. Shekhar, Y. Sun, V. Sü, M. Schmidt, U. Schwarz, E. Pippel, P. Werner, R. Hillebrand, T. Förster, E. Kampert, S. Parkin, R. J. Cava, C. Felser, B. Yan and S. A. Medvedev, Superconductivity in Weyl Semimetal Candidate MoTe$_2$, *Nat. Commun.*, 2016, **7**, 11038.

7 S. Cho, S. H. Kang, H. S. Yu, H. W. Kim, W. Ko, S. W. Hwang, W. H. Han, D. Choe, Y. H. Jung, K. J. Chang, Y. H. Lee, H. Yang and S. W. Kim, Te Vacancy-Driven Superconductivity in Orthorhombic Molybdenum Ditelluride, *2D Mater.*, 2017, **4**, 021030.

8 W. Wang, S. Kim, M. Liu, F. A. Cevallos, R. J. Cava and N. P. Ong, Evidence for an Edge Supercurrent in the Weyl Superconductor MoTe$_2$, *Science*, 2020, **368**, 534–537.

9 X. Qian, J. Liu, L. Fu and J. Li, Quantum Spin Hall Effect in Two-Dimensional Transition Metal Dichalcogenides, *Science*, 2014, **346**, 1344–1347.

10 W. Hou, A. Azizimanesh, A. Sewaket, T. Peña, C. Watson, M. Liu, H. Askari and S. M. Wu, Strain-Based Room-Temperature Non-Volatile MoTe$_2$ Ferroelectric Phase Change Transistor, *Nat. Nanotechnol.*, 2019, **14**, 668–673.

11 Y. Wang, J. Xiao, H. Zhu, Y. Li, Y. Alsaid, K. Y. Fong, Y. Zhou, S. Wang, W. Shi, Y. Wang, A. Zettl, E. J. Reed and X. Zhang, Structural Phase Transition in Monolayer MoTe$_2$ Driven by Electrostatic Doping, *Nature*, 2017, **550**, 487–491.

12 C. Zhang, S. KC, Y. Nie, C. Liang, W. G. Vandenberghe, R. C. Longo, Y. Zheng, F. Kong, S. Hong, R. M. Wallace and K. Cho, Charge Mediated Reversible Metal–Insulator Transition in Monolayer MoTe$_2$ and W$_x$Mo$_{1-x}$Te$_2$ Alloy, *ACS Nano*, 2016, **10**, 7370–7375.

13 M. J. Mleczko, A. C. Yu, C. M. Smyth, V. Chen, Y. C. Shin, S. Chatterjee, Y. C. Tsai, Y. Nishi, R. M. Wallace and E. Pop, Contact Engineering High-Performance n-Type MoTe$_2$ Transistors, *Nano Lett.*, 2019, **19**, 6352–6362.

14 N. R. Pradhan, D. Rhodes, S. Feng, Y. Xin, S. Memaran, B. H. Moon, H. Terrones, M. Terrones and L. Balicas, Field-Effect Transistors Based on Few-Layered α-MoTe$_2$, *ACS Nano*, 2014, **8**, 5911–5920.

15 D. J. Hynek, R. M. Singhania, S. Xu, B. Davis, L. Wang, M. Yarali, J. V. Pondick, J. M. Woods, N. C. Strandwitz and J. J.

Cha, Cm$^2$-Scale Synthesis of MoTe$_2$ Thin Films with Large Grains and Layer Control, *ACS Nano*, 2021, **15**, 410–418.

16 C. Ruppert, O. B. Aslan and T. F. Heinz, Optical Properties and Band Gap of Single- and Few-Layer MoTe$_2$ Crystals, *Nano Lett.*, 2014, **14**, 6231–6236.

17 M. Grzeszczyk, K. Gołasa, M. Zinkiewicz, K. Nogajewski, M. R. Molas, M. Potemski, A. Wysmołek and A. Babiñski, Raman Scattering of Few-Layers MoTe$_2$, *2D Mater.*, 2016, **3**, 025010.

18 Q. J. Song, Q. H. Tan, X. Zhang, J. B. Wu, B. W. Sheng, Y. Wan, X. Q. Wang, L. Dai and P. H. Tan, Physical Origin of Davydov Splitting and Resonant Raman Spectroscopy of Davydov Components in Multilayer MoTe$_2$, *Phys. Rev. B*, 2016, **93**, 115409.

19 J. Wang, X. Luo, S. Li, I. Verzhbitskiy, W. Zhao, S. Wang, S. Y. Quek and G. Eda, Determination of Crystal Axes in Semimetallic T'-MoTe$_2$ by Polarized Raman Spectroscopy, *Adv. Funct. Mater.*, 2017, **27**, 1604799.

20 J.-H. Huang, H.-H. Hsu, D. Wang, W.-T. Lin, C.-C. Cheng, Y.-J. Lee and T.-H. Hou, Polymorphism Control of Layered MoTe$_2$ through Two-Dimensional Solid-Phase Crystallization, *Sci. Rep.*, 2019, **9**, 8810.

21 W. Xu, J. Yan, N. Wu, H. Zhang, Y. Xie, Y. Tang, Y. Zhu and W. Yao, Diffusing Behavior of MoO$_3$ on Al$_2$O$_3$ and SiO$_2$ Thin Films, *Surf. Sci.*, 2000, **470**, 121–130.

22 B. Groven, A. N. Mehta, H. Bender, Q. Smets, J. Meersschaut, A. Franquet, T. Conard, T. Nuytten, P. Verdonck, W. Vandervorst, M. Heyns, I. Radu, M. Caymax and A. Delabie, Nucleation Mechanism during WS$_2$ Plasma Enhanced Atomic Layer Deposition on Amorphous Al$_2$O$_3$ and Sapphire Substrates, *J. Vac. Sci. Technol., A*, 2018, **36**, 01A105.

23 B. Groven, A. Nalin Mehta, H. Bender, J. Meersschaut, T. Nuytten, P. Verdonck, T. Conard, Q. Smets, T. Schram, B. Schoenaers, A. Stesmans, V. Afanas'Ev, W. Vandervorst, M. Heyns, M. Caymax, I. Radu and A. Delabie, Two-Dimensional Crystal Grain Size Tuning in WS$_2$ Atomic Layer Deposition: An Insight in the Nucleation Mechanism, *Chem. Mater.*, 2018, **30**, 7648–7663.

24 S. L. Hemmingson and C. T. Campbell, Trends in Adhesion Energies of Metal Nanoparticles on Oxide Surfaces: Understanding Support Effects in Catalysis and Nanotechnology, *ACS Nano*, 2017, **11**, 1196–1203.

25 G. H. Ahn, M. Amani, H. Rasool, D. H. Lien, J. P. Mastandrea, J. W. Ager, M. Dubey, D. C. Chrzan, A. M. Minor and A. Javey, Strain-Engineered Growth of Two-Dimensional Materials, *Nat. Commun.*, 2017, **8**, 608.

26 S. Song, D. H. Keum, S. Cho, D. Perello, Y. Kim and Y. H. Lee, Room Temperature Semiconductor−Metal Transition of MoTe$_2$ Thin Films Engineered by Strain, *Nano Lett.*, 2016, **16**, 188–193.

27 D. Zhang, Y. Wang and Y. Gan, Characterization of Critically Cleaned Sapphire Single-Crystal Substrates by Atomic Force Microscopy, XPS and Contact Angle Measurements, *Appl. Surf. Sci.*, 2013, **274**, 405–417.

28 A. Bertuch, G. Sundaram, M. Saly, D. Moser and R. Kanjolia, Atomic Layer Deposition of Molybdenum Oxide Using Bis(Tert-Butylimido)Bis(Dimethylamido) Molybdenum, *J. Vac. Sci. Technol., A*, 2014, **32**, 01A119.